inorganics

MDPI

Article

Heteroleptic [Cu(P^P)(N^N)][PF_6] Compounds with Isomeric Dibromo-1,10-Phenanthroline Ligands

Isaak Nohara, Aramis Keller, Nikolai Tarassenko, Alessandro Prescimone, Edwin C. Constable and Catherine E. Housecroft *

Department of Chemistry, University of Basel, BPR 1096, Mattenstrasse 24a, 4058 Basel, Switzerland; isaak.nohara@unibas.ch (I.N.); aramis.keller@stud.unibas.ch (A.K.); nikolai.tarassenko@stud.unibas.ch (N.T.); alessandro.prescimone@unibas.ch (A.P.); edwin.constable@unibas.ch (E.C.C.)

* Correspondence: catherine.housecroft@unibas.ch

Received: 4 December 2019; Accepted: 8 January 2020; Published: 10 January 2020

Abstract: A series of [Cu(P^P)(N^N)][PF_6] compounds are reported in which N^N is 2,9-dibromo-1,10-phenanthroline (2,9-Br_2phen), 3,8-dibromo-1,10-phenanthroline (3,8-Br_2phen) or 4,7-dibromo-1,10-phenanthroline (4,7-Br_2phen) and P^P is bis(2-(diphenylphosphano)phenyl)ether (POP) or 4,5-bis (diphenylphosphano)-9,9-dimethylxanthene (xantphos). The compounds were characterized by solution multinuclear NMR spectroscopy, mass spectrometry and a single-crystal X-ray analysis. Each compound underwent a partially reversible or irreversible copper-centred oxidation, the highest potential being for 2,9-Br_2phen-containing compounds. In solution, the compounds are weak yellow or orange emitters, whereas powdered samples exhibit yellow emissions with photoluminescence quantum yields of up to 45% for [Cu(xantphos)(2,9-Br_2phen)][PF_6] with an excited state lifetime $\tau_{1/2}$ = 9.9 μs. Values of $\lambda_{em}{}^{max}$ for [Cu(POP)(2,9-Br_2phen)][PF_6] and [Cu(xantphos)(2,9-Br_2phen)][PF_6] are blue-shifted with respect to compounds with the 3,8-and 4,7-isomers, both in solution and in the solid state.

Keywords: copper(I); 1,10-phenanthroline; bromo-substitution; photophysical properties

1. Introduction

The ground-breaking work of McMillin and coworkers [1,2] paved the way to the understanding and subsequent exploitation of the photoluminescent behaviour of the metal-to-ligand charge transfer (MLCT) state of heteroleptic copper(I) coordination compounds containing 1,10-phenanthroline (phen) or 2,2′-bipyridine (bpy) combined with phosphane or bis(phosphane) ligands. More recently, it has emerged that these [Cu(P^P)(N^N)]$^+$ complexes exhibit thermally activated delayed fluorescence (TADF) [3–5], a phenomenon in which the first excited singlet state is populated by a thermally activated transition from the first excited triplet state resulting in a corresponding improvement in the emission properties of the compounds. As a consequence, [Cu(P^P)(N^N)]$^+$ compounds are of significant interest for application in light-emitting electrochemical cells (LECs) which represent a potential new approach to the development of solid-state lighting technologies [6–8]. LECs based on ionic transition-metal complexes (iTMCs) have conventionally been based on ruthenium(II) or iridium(III) compounds [6,9]. These heavier *d*-block metals were initially selected because the large spin-orbit coupling leads to singlet-triplet mixing, consequently allowing harvesting of both singlet and triplet excitons [6]. However, interest in copper-based iTMCs has grown [10–12], motivated, in part, by the lower cost and higher natural abundance of copper with respect to the heavier *d*-block metal, and the opportunity to harvest all spin-states through a TADF mechanism.

Of the mononuclear [Cu(P^P)(N^N)]$^+$ complexes reported to date, the most common P^P ligands are xantphos (4,5-bis(diphenylphosphano)-9,9-dimethylxanthene, IUPAC PIN (9,9-dimethyl-9*H*-xanthene-

4,5-diyl)bis(diphenylphosphane)) and POP (bis(2-(diphenylphosphano)phenyl)ether, IUPAC PIN oxydi(2,1-phenylene)bis(diphenylphosphane)) (Scheme 1). The majority of the N^N ligands possess a bpy or phen metal-binding domain. We have focused on bpy-derived ligands and have shown that 6-alkyl, 6,6′-dialkyl or 6-alkyloxy substituted bpy ligands with sterically non-demanding groups lead to some of the best-performing LECs [10,13,14]. These conclusions are further supported by the results of Costa, Barolo and coworkers, who have demonstrated the beneficial effects of using the 6,6′-dimethoxy-2,2′-bipyridine ligand in $[Cu(POP)(N^N)]^+$ emitters [15]. Our investigations of $[Cu(POP)(N^N)]^+$ and $[Cu(xantphos)(N^N)]^+$ complexes containing 6-halo- and 6,6′-dihalo-2,2′-bipyridine ligands have shown that Cl and Br atoms are less effective than methyl groups in the enhancement of the emission of $[Cu(P^P)(bpy)][PF_6]$ compounds. Nonetheless, several of these halo-containing compounds exhibit moderately good photophysical properties with $[Cu(xantphos)(6\text{-}Brbpy)][PF_6]$, $[Cu(POP)(6,6'\text{-}Cl_2bpy)][PF_6]$, $[Cu(xantphos)(6,6'\text{-}Cl_2bpy)][PF_6]$ showing photoluminescence quantum yields (PLQYs) of 16.3%, 14.8% and 17.1%, respectively, in the solid state [16]. LECs with $[Cu(POP)(6,6'\text{-}Cl_2bpy)][PF_6]$ and $[Cu(xantphos)(6,6'\text{-}Cl_2bpy)][PF_6]$ in the emissive layer have turn-on times of <12 s and exhibit maximum luminances of 121 and 259 cd m^{-2}, respectively [16].

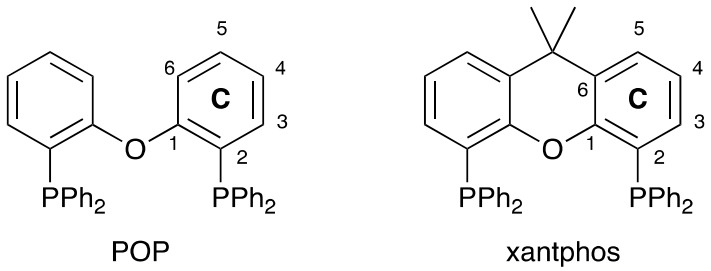

Scheme 1. Structures of POP and xantphos. Atom labels are used for the NMR spectroscopic assignments; phenyl rings in the PPh_2 units are labelled D, and ring labels are consistent with our previous publications in this area.

In solution, dynamic ligand redistribution is often a problem with heteroleptic $[Cu(P^P)(N^N)]^+$ compounds, resulting in mixtures containing both the heteroleptic complex and the homoleptic $[Cu(N^N)_2]^+$ and $[Cu(P^P)_2]^+$ species (Equation (1)). When P^P is bulky, as in the case of POP, three coordinate $[Cu(P^P)(solv)]^+$ (solv = solvent such as MeCN) complexes may also be formed [17]. When N^N is a bpy-derivative, synthetic strategies can be adapted to favour the formation of the heteroleptic compounds [18,19]. For N^N ligands based upon phen metal-binding domains, Armaroli, Nierengarten, Delavaux-Nicot and coworkers have carried out detailed investigations of the ligand redistribution reactions occurring in $[Cu(P^P)(N^N)]^+$ complexes, and have demonstrated that 2,9-substituted phen ligands favour the right-hand side of equilibrium (1) unless the P^P ligand is sterically hindered (e.g., POP) [20]. They have also provided valuable insight into structure–property relationships for a series of $[Cu(P^P)(phen)]^+$ and $[Cu(P^P)(4,7\text{-}Ph_2phen)]^+$ (4,7-Ph_2phen = 4,7-diphenyl-1,10-phenanthroline) [11]. In particular, they observed that the larger the number of intramolecular π-interactions in the ground-state complex, the higher the PLQY. The presence of these π-interactions restricts the flattening of the copper coordination sphere in the excited state. Phenomenologically, this parallels the beneficial effects of intramolecular π-interactions observed in cyclometallated iridium(III) emitters [21,22].

$$2[Cu(P^P)(N^N)]^+ \rightleftharpoons [Cu(N^N)_2]^+ + [Cu(P^P)_2]^+ \quad (1)$$

While a range of $[Cu(P^P)(N^N)]^+$ complexes with alkyl- or aryl-substituted phen ligands has been investigated [12], there are few reports of $[Cu(P^P)(N^N)]^+$ complexes containing simple halo-substituted phen ligands. The study of chelating bisphosphane ligands arose from the observations of Casadonte and McMillin who demonstrated non-equilibrated emissions from

two triplet excited states in a series of compounds, including $[Cu(PPh_3)_2(5\text{-Clphen})][BF_4]$ and $[Cu(PPh_3)_2(4,7\text{-}Cl_2phen)][BF_4]$ in a 4:1 EtOH/MeOH frozen glass at 77 K [23]. Further examples come from more recent investigations. Solid $[Cu(bdpp)(phen)][ClO_4]$ and $[Cu(bdpp)(3,8\text{-}Br_2phen)][ClO_4]$ (bdpp = 1,2-bis(diphenylphosphane)benzene, and 3,8-Br_2phen is shown in Scheme 2) emit at 553 and 570 nm, respectively (λ_{exc} = 300–430 nm) with PLQY values of 18.33% and 3.58%, respectively [24]. Xin et al. have reported that in the solid state, the dinuclear compounds $[(3,8\text{-}Br_2phen)Cu(\mu\text{-}Ph_2P(CH_2)_nPPh_2)_2Cu(3,8\text{-}Br_2phen)][ClO_4]_2$ exhibit emission maxima at 543, 565, 559 and 566 nm for n = 1, 4, 5 and 6, respectively (λ_{exc} = 330 nm); for n = 5, the PLQY value is 17.4%. These compounds emit weakly in CH_2Cl_2 solution, but in mixtures of CH_2Cl_2 and hexane, they exhibit aggregation-induced phosphorescent emission [25]. Feng et al. [26] have demonstrated that $[Cu(xantphos)(3,8\text{-}Br_2phen)][ClO_4]$ and $[Cu(BINAP)(3,8\text{-}Br_2phen)][ClO_4]$ (BINAP = 2,2′-bis(diphenylphosphano)-1,1′-binaphthalene) are emissive in the solid state (λ_{exc} = 365 nm), but no PLQY values were reported. A recent investigation of the impact of halo-substituents on the photophysical behaviour of the homoleptic complexes $[Cu(2,9\text{-}X_2phen)_2][PF_6]$ where X = Cl, Br or I is also relevant. This reveals that for X = Br and I, PLQY values for $[Cu(2,9\text{-}X_2phen)_2][PF_6]$ are higher than for $[Cu(phen)_2][PF_6]$. Significantly, whereas $[Cu(2,9\text{-}Cl_2phen)_2][PF_6]$ and $[Cu(2,9\text{-}Br_2phen)_2][PF_6]$ exhibit TADF, for $[Cu(2,9\text{-}I_2phen)_2][PF_6]$ the PLQY increases as temperature decreases as a consequence of the system being efficiently trapped in a C_2-symmetric singlet excited state [27].

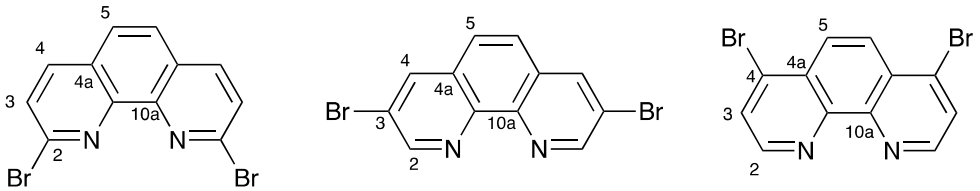

Scheme 2. Structures of the N^N ligands, with atom labels used for the NMR spectroscopic assignments (the phen rings are labelled A).

We now report an extension of our earlier investigation of $[Cu(POP)(N^N)]^+$ and $[Cu(xantphos)(N^N)]^+$ complexes containing 6-halo- and 6,6′-dihalo-2,2′-bipyridine ligands [16] to a series of $[Cu(POP)(Br_2phen)][PF_6]$ and $[Cu(xantphos)(Br_2phen][PF_6]$ compounds in which Br_2phen represents the three isomers shown in Scheme 2.

2. Results and Discussion

2.1. Synthesis and Characterization of Copper(I) Complexes

We have previously discussed the need for different strategies for the preparations of $[Cu(POP)(N^N][PF_6]$ and $[Cu(xantphos)(N^N][PF_6]$ compounds in which the N^N ligand is a derivative of bpy [10,14]. Similarly, different approaches were used to optimize the yields of the heteroleptic copper(I) complexes containing the dibromophen ligands and either POP or xantphos. $[Cu(POP)(2,9\text{-}Br_2phen)][PF_6]$, $[Cu(POP)(3,8\text{-}Br_2phen)][PF_6]$ and $[Cu(POP)(4,7\text{-}Br_2phen)][PF_6]$ were prepared by first combining POP and $[Cu(MeCN)_4][PF_6]$ in CH_2Cl_2 and then, after stirring for an hour, adding the appropriate Br_2phen. In contrast, the series of $[Cu(xantphos)(Br_2phen)][PF_6]$ compounds were synthesized by adding a CH_2Cl_2 solution of xantphos and either 2,9-Br_2phen, 3,8-Br_2phen or 4,7-Br_2phen to a CH_2Cl_2 solution of $[Cu(MeCN)_4][PF_6]$ and stirring at room temperature for 90 min. Each product was purified by crystallization by vapour diffusion of Et_2O into a CH_2Cl_2 solution of the crude material.

Satisfactory elemental analyses were obtained for all the heteroleptic copper(I) complexes expect for [Cu(POP)(2,9-Br2phen)][PF6], and for the latter, a high-resolution electrospray (HR ESI) mass spectrum was recorded (Figure S1, see Supporting Information). The electrospray mass spectrum of

each of [Cu(POP)(2,9-Br2phen)][PF6], [Cu(POP)(3,8-Br2phen)][PF6] and [Cu(POP)(4,7-Br2phen)][PF6] exhibited a peak corresponding to the [M − PF6]+ ion at m/z 939.02, 938.96 and 938.98, respectively (Figures S2–S4). For [Cu(POP)(2,9-Br2phen)][PF6], the base peak was observed at m/z 601.09 and was assigned to the [Cu(POP)]+ ion (Figure S2), whereas in the mass spectra of the compounds containing 3,8-Br2phen and 4,7-Br2phen, the peak for the [Cu(POP)]+ ion (m/z 601.06 and 601.011, respectively) was of low intensity. Similarly, the base peak in the ESI mass spectrum of [Cu(xantphos)(2,9-Br2phen)][PF6] arose from the [Cu(xantphos)]+ ion (m/z 641.13), with the [M − PF6]+ ion giving a lower intensity peak at m/z 979.03 (Figure S5). In the mass spectra of [Cu(xantphos)(3,8-Br2phen)][PF6] and [Cu(xantphos)(4,7-Br2phen)][PF6], the peak arising from the [M − PF6]+ ion (m/z 979.03 and 979.00, respectively, Figures S6 and S7) was of significantly greater intensity than that assigned to the [Cu(xantphos)]+ ion (m/z 641.12 and 641.15, respectively). These differences may be attributed to the steric effects of the 2,9-dibromo substituents compared to the 3,8- and 4,7-substitution pattern, and are manifested in the crystallographic data discussed later.

The solution ^{1}H, ^{13}C{^{1}H} and ^{31}P{^{1}H} NMR spectra of the copper(I) complexes were recorded in acetone-d_6. Each ^{31}P{^{1}H} NMR spectrum exhibited a broadened singlet in the range δ −10.1 to −12.4 ppm (see Methods and Materials Section) arising from the POP or xantphos ligand, in addition to a septet at δ −144.2 ppm assigned to the $[PF_6]^-$ ion. The ^{1}H and ^{13}C{^{1}H} NMR spectra were assigned using COSY, NOESY, HMQC and HMBC methods and Figures S8–S25 show the ^{1}H NMR, HMQC and HMBC spectra. As a representative example, the aromatic regions of the ^{1}H NMR spectra of [Cu(POP)(3,8-Br_2phen)][PF_6] and [Cu(xantphos)(3,8-Br_2phen)][PF_6] are compared in Figure 1. The change in the multiplicity of the signal for H^{C5} and the disappearance of the signal for H^{C6} on going from [Cu(POP)(3,8-Br_2phen)][PF_6] to [Cu(xantphos)(3,8-Br_2phen)][PF_6] is consistent with the introduction of the CMe_2 unit in xantphos (see Scheme 1). The methyl groups of the CMe_2 group give rise to a singlet at δ 1.74 ppm in [Cu(xantphos)(2,9-Br_2phen)][PF_6], at δ 1.87 ppm in [Cu(xantphos)(3,8-Br_2phen)][PF_6] and at δ 1.81 ppm in [Cu(xantphos)(4,7-Br_2phen)][PF_6]. In contrast to the solid-state structures described below, the molecular symmetry inferred from the room temperature ^{1}H, ^{13}C{^{1}H} and ^{31}P{^{1}H} NMR spectra is consistent with dynamic behaviour analogous to that described for related bpy-containing compounds [14,19]. A comparison of Figure 1a with Figure 1b reveals that the signal for proton H^{A2} undergoes a significant shift to lower frequency on going from [Cu(POP)(3,8-Br_2phen)][PF_6] to [Cu(xantphos)(3,8-Br_2phen)][PF_6]. This is a consequence of the proximity of H^{A2} to the xanthene unit which has a "bowl" conformation (see the structural discussion of [Cu(xantphos)(3,8-Br_2phen)][PF_6] below). Inversion of the "bowl" [14,19] renders the phenanthroline unit C_2 symmetric on the NMR timescale at room temperature with both H^{A2} protons experiencing the effects of being positioned over the xanthene unit. We have seen similar effects in [Cu(xantphos)(6-Rbpy)]$^+$ compounds in which proton H^{A6} (which is in the unsubstituted pyridine ring and is adjacent to the N atom) appears at very different chemical shifts, depending on whether it is located over or remote from the xanthene "bowl" [14,19].

Since the solution photophysical and electrochemical properties of the compounds were investigated in CH_2Cl_2, we confirmed the stability of the heteroleptic complexes in this solvent. The ^{1}H NMR spectrum of a CD_2Cl_2 solution of [Cu(POP)(4,7-Br_2phen)][PF_6] did not change over a period of 6 h at room temperature (Figure S26a). In the NOESY spectrum (Figure S26b), a cross peak between signals for protons H^{A2} (on the 4,7-Br_2phen ligand) and H^{D2} (on POP) confirms the heteroleptic nature of the complex.

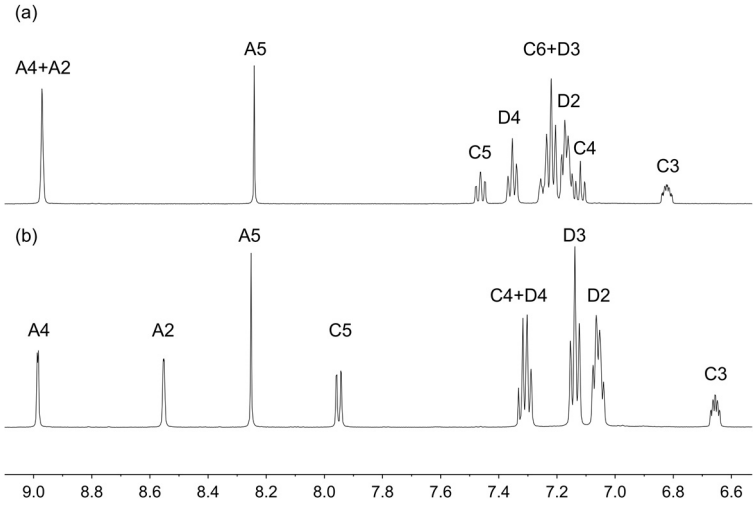

Figure 1. The aromatic region of the ^{1}H NMR spectra (500 MHz, acetone-d_6, 298 K) of (**a**) [Cu(POP)(3,8-Br$_2$phen)][PF$_6$] and (**b**) [Cu(xantphos)(3,8-Br$_2$phen)][PF$_6$]. See Schemes 1 and 2 for atom labels. Chemical shifts in δ/ppm.

2.2. Crystal Structures

Yellow single crystals of [Cu(POP)(2,9-Br$_2$phen)][PF$_6$]·0.5Et$_2$O, [Cu(POP)(3,8-Br$_2$phen)][PF$_6$]·0.8CH$_2$Cl$_2$·0.9H$_2$O, [Cu(POP)(4,7-Br$_2$phen)][PF$_6$]·CH$_2$Cl$_2$, [Cu(xantphos)(2,9-Br$_2$phen)][PF$_6$]·1.1CH$_2$Cl$_2$, [Cu(xantphos)(3,8-Br$_2$phen)][PF$_6$]·1.1CH$_2$Cl$_2$·0.7Et$_2$O and [Cu(xantphos)(4,7-Br$_2$phen)][PF$_6$]·CH$_2$Cl$_2$·0.9Et$_2$O were grown from CH$_2$Cl$_2$ solutions of the compounds layered with Et$_2$O. In [Cu(xantphos)(2,9-Br$_2$phen)][PF$_6$]·1.1CH$_2$Cl$_2$, the xantphos ligand is disordered and has been modelled over two sites of equal occupancies, the sites of the xanthene unit being related by a mirror plane. The asymmetric unit contains half of the 2,9-Br$_2$phen ligand and the second half is generated by a mirror plane. Associated with this is the disorder of three of the four phenyl rings of the PPh$_2$ units. Because of the extent of disorder, we will not discuss this structure in detail but merely comment that it provides confirmation that the 2,9-Br$_2$phen ligand is present in a chelating mode despite the steric hindrance of the two bromo-substituents adjacent to the N-donors. The structures of the [Cu(P^P)(N^N)]$^+$ cations in the remaining structures are displayed in Figures 2 and 3. A comparison of the Cu–N and Cu–P bond lengths and of the N–Cu–N and P–Cu–P bond angles is provided in Table 1. Because of the rigidity of the chelating phen unit, the N–Cu–N angle is close to 80° in all structures. The POP ligand is conformationally flexible and the P–Cu–P bond angle ranges from 118.00(3)° to 112.37(2)°, the angle becoming smaller along the series 2,9-Br$_2$phen > 3,8-Br$_2$phen > 4,7-Br$_2$phen (Table 1). The same trend is observed for the xantphos-containing cations, although the range of angles is smaller (Table 1). The distorted 4-coordinate geometry of the copper(I) atom in each complex cation is typical of heteroleptic [Cu(P^P)(N^N)]$^+$ complexes. Using Houser's τ_4 parameter [28], the values of 0.83 to 0.88 (Table 1) illustrate distortion towards C_{3v} symmetry for which τ_4 = 0.85; for T_d symmetry, τ_4 = 1.00. We note that the unit cell dimensions for [Cu(POP)(2,9-Br$_2$phen)][PF$_6$]·Et$_2$O (see the Materials and Methods section) are very similar to those reported for [Cu(POP)(2,9-Me$_2$phen)][PF$_6$]·Et$_2$O [29] (Cambridge Strucural Database, CSD, refcode CAPZID [30]).

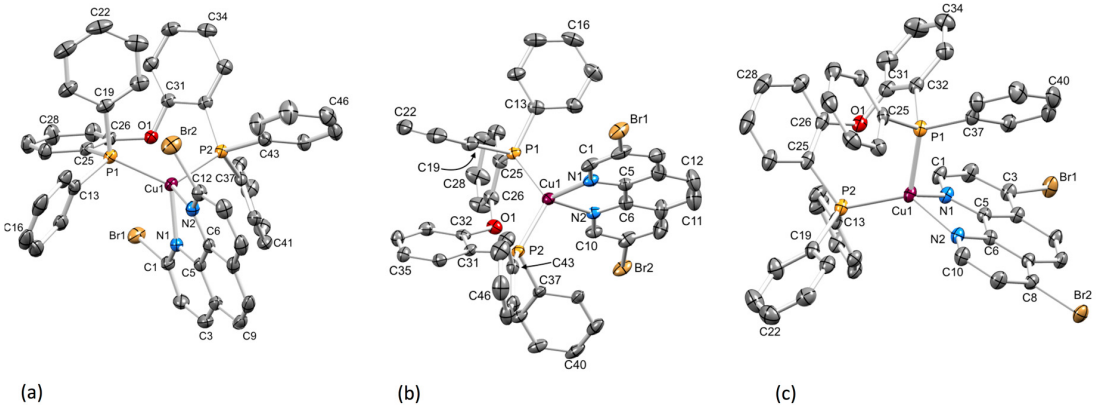

Figure 2. The structures of the POP-containing cations with H atoms omitted. (**a**) [Cu(POP)(2,9-Br_2phen)]$^+$ (ellipsoids plotted at 50% probability), (**b**) [Cu(POP)(3,8-Br_2phen)]$^+$ (ellipsoids plotted at 40% probability) and (**c**) [Cu(POP)(4,7-Br_2phen)]$^+$ (ellipsoids plotted at 50% probability). In [Cu(POP)(2,9-Br_2phen)][PF_6]·0.5Et_2O and [Cu(POP)(4,7-Br_2phen)][PF_6]·CH_2Cl_2, there are two independent ions pairs in the asymmetric unit and only one cation is shown (see also Table 1 and the accompanying discussion).

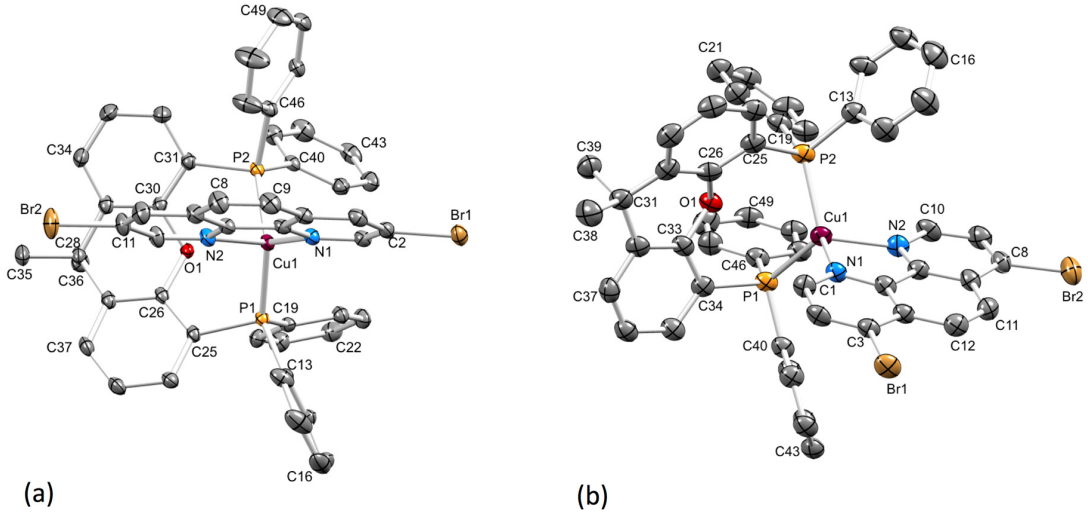

Figure 3. The structures of the cations in [Cu(xantphos)(3,8-Br_2phen)][PF_6]·1.1CH_2Cl_2·0.7Et_2O and [Cu(xantphos)(4,7-Br_2phen)][PF_6]·CH_2Cl_2·0.9Et_2O with ellipsoids plotted at 40% probability level and H atoms omitted for clarity. (**a**) [Cu(xantphos)(3,8-Br_2phen)]$^+$ and (**b**) [Cu(xantphos)(4,7-Br_2phen)]$^+$.

Table 1. Comparison of the bond lengths and angles in the coordination spheres of the [Cu(P^P)(N^N)][PF_6] complexes.

[Cu(P^P)(N^N)]$^+$ Cation [1]	Cu–N/Å	Cu–P/Å	P–Cu–P/Deg	N–Cu–N/Deg	τ_4 [2]
[Cu(POP)(2,9-Br_2phen)]$^+$ Cation 1	2.100(2), 2.135(2)	2.2742(7), 2.2416(7)	118.00(3)	79.61(8)	0.87
[Cu(POP)(2,9-Br_2phen)]$^+$ Cation 2	2.149(2), 2.129(2)	2.2849(7), 2.2704(7)	116.47(3)	78.46(9)	0.87
[Cu(POP)(3,8-Br_2phen)]$^+$	2.055(6), 2.083(5)	2.2468(17), 2.2332(18)	115.65(7)	80.9(2)	0.88
[Cu(POP)(4,7-Br_2phen)]$^+$ Cation 1	2.0797(19), 2.0607(19)	2.2622(7), 2.2377(7)	112.37(2)	80.22(7)	0.84
[Cu(POP)(4,7-Br_2phen)]$^+$ Cation 2	2.088(2), 2.0683(19)	2.2694(7), 2.2370(7)	112.52(3)	80.34(8)	0.85
[Cu(xantphos)(2,9-Br_2phen)]$^+$	2.115(4), 2.115(4) [3]	2.295(2), 2.2523(18)	117.97(8)	79.2(2)	0.83
[Cu(xantphos)(3,8-Br_2phen)]$^+$	2.079(2), 2.122(2)	2.2495(7), 2.2752(7)	116.57(3)	80.45(8)	0.87
[Cu(xantphos)(4,7-Br_2phen)]$^+$	2.075(4), 2.069(5)	2.2619(15), 2.2591(15)	115.36(6)	80.29(16)	0.87

[1] In[Cu(POP)(2,9-Br_2phen)][PF_6]·0.5Et_2O and [Cu(POP)(4,7-Br_2phen)][PF_6]·CH_2Cl_2, there are two independent ions pairs in the asymmetric unit. [2] τ_4 parameter, see reference [28]. [3] The N atoms are symmetry-related (symmetry code x, 1−y, z).

The asymmetric units in [Cu(POP)(2,9-Br_2phen)][PF_6]·0.5Et_2O and [Cu(POP)(4,7-Br_2phen)][PF_6]·CH_2Cl_2 contain two independent ion-pairs. The bond parameters in the coordination spheres of the copper centres are similar (Table 1). Figure 4 illustrates an overlay of the independent [Cu(POP)(4,7-Br_2phen)]$^+$ cations with the POP ligands approximately superimposed.

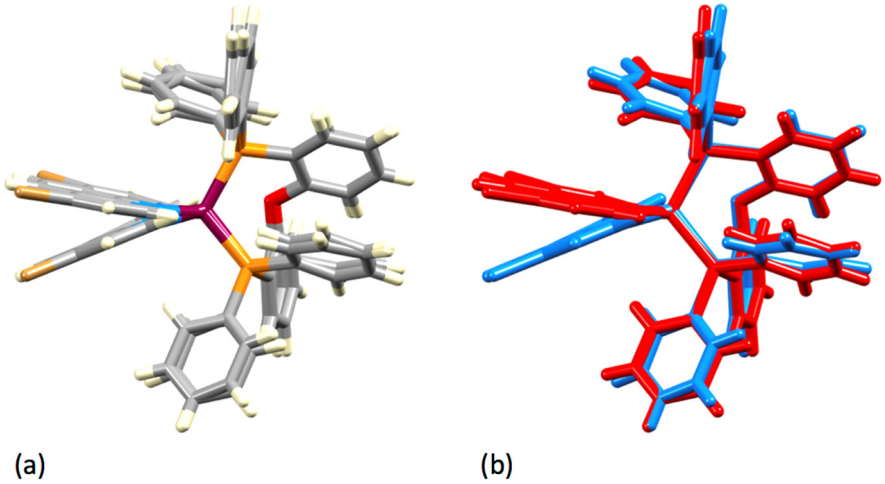

Figure 4. Overlay of the two independent cations in [Cu(POP)(4,7-Br_2phen)][PF_6]·CH_2Cl_2: (**a**) coloured by element colour, and (**b**) coloured to show the individual cations.

In the solid state, [Cu(POP)(N^N)]$^+$ and [Cu(xantphos)(N^N)]$^+$ cations often exhibit intra-cation π-stacking contacts. [Cu(POP)(N^N)]$^+$ cations tend to show face-to-face π-stacking between one phenyl ring of a PPh_2 unit and one arene ring of the POP backbone, while face-to-face π-stacking between two phenyl rings of different PPh_2 units is often a feature of [Cu(xantphos)(N^N)]$^+$ cations, see for example [10]. The cations in [Cu(POP)(3,8-Br_2phen)][PF_6] and [Cu(POP)(4,7-Br_2phen)][PF_6] all show π-stacking between one phenyl ring and the POP backbone (Figure 5) with angles between the ring planes of 27.7 (Figure 5a), 27.9 and 17.1° (Figure 5b) and centroid distances 4.1, 4.0 and 3.8 Å, respectively. No analogous interaction is observed in [Cu(POP)(2,9-Br_2phen)][PF_6], and a contributing factor may be the effects that the bromo-substituents in the 2,9-positions have on the orientations of the phenyl rings. We note, however, that the cations are closely associated in the solid state structure, as exemplfied for [Cu(POP)(2,9-Br_2phen)][PF_6]·0.5Et_2O in Figure 6, and there is clearly an interplay of intra- and inter-cation interactions in all the structures. Intra-cation π-stacking is observed in the [Cu(xantphos)(4,7-Br_2phen)]$^+$ cation as shown in Figure 5c; the interaction is characterized by an angle of 28° between the planes of the phenyl rings and a centroid···centroid distance of 4.0 Å.

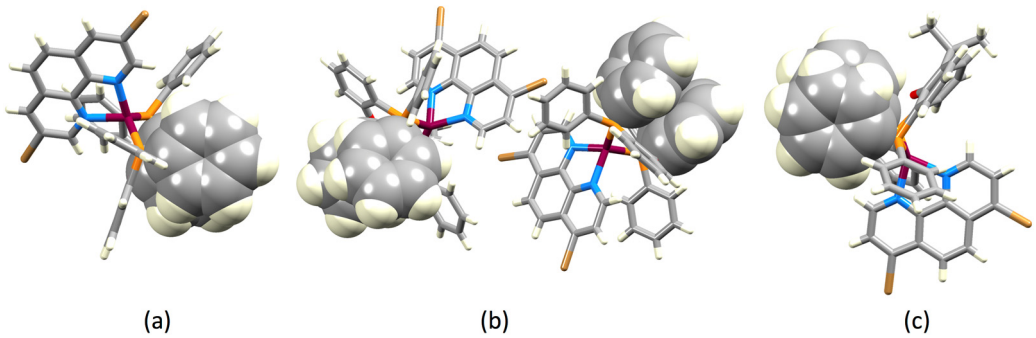

Figure 5. Space-filling representations of the π-stacking between one phenyl ring of a PPh_2 unit and one arene ring of the POP backbone in (**a**) [Cu(POP)(3,8-Br_2phen)]$^+$ and (**b**) the independent [Cu(POP)(4,7-Br_2phen)]$^+$ cations. (**c**) Space-filling representation of the π-stacking between two phenyl rings of different PPh_2 units in [Cu(xantphos)(4,7-Br_2phen)]$^+$.

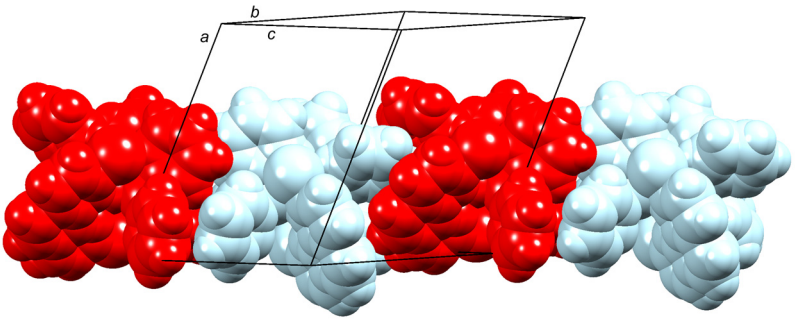

Figure 6. Packing of independent cations (red and pale blue) into chains in [Cu(POP)(2,9-Br_2phen)][PF_6]·0.5Et_2O shown in space-filling representation. Anions and solvent molecules are omitted.

2.3. Electrochemistry

Cyclic voltammograms (CVs) of CH_2Cl_2 solutions of the [Cu(P^P)(N^N)][PF_6] compounds were recorded and Table 2 gives the potentials of the electrochemical processes. Each compound undergoes a partially-reversible or irreversible oxidation assigned to a Cu^+/Cu^{2+} process. The degree of reversiblity for [Cu(POP)(3,8-Br_2phen)][PF_6], [Cu(POP)(4,7-Br_2phen)][PF_6] and [Cu(xantphos)(2,9-Br_2phen)][PF_6] is demonstrated by the I_{pc}/I_{pa} ratios in Table 2. We note that changing the solvent from CH_2Cl_2 to 4-methyl-1,3-dioxolan-2-one (propylene carbonate) did not improve the reversiblity of the Cu^+/Cu^{2+} processes. If the forward CV scan is taken beyond +1.2 V, a second (fully irreversible) process is observed around +1.3 V and this is assigned to phosphane oxidation. A representative CV is shown in Figure S27, and anodic and cathodic scans for all the compounds are displayed in Figures S28–S33. The copper(I) oxidation occurs at highest potentials for [Cu(POP)(2,9-Br_2phen)][PF_6] and [Cu(xantphos)(2,9-Br_2phen)][PF_6], consistent with the steric effects of the bromo-substituents in the 2,9-positions which hinder flattening of the copper coordination sphere during oxidation. The same trend is observed on going from [Cu(POP)(phen)][BF_4] to [Cu(POP)(2,9-Me_2phen)][BF_4] for the which the Cu^+/Cu^{2+} oxidation occurs at +1.23 V and +1.38 V, respectively (referenced with respect to Ag/AgCl) [31]. Similarly, the introduction of chloro- or bromo-substituents into the 6- and 6′-positions of bpy in [Cu(POP)(bpy)][PF_6] or [Cu(xantphos)(bpy)][PF_6] shifts the Cu^+/Cu^{2+} oxidation from +0.72 or +0.76 V to +0.98 or +0.93 V, respectively for 6,6′-Cl_2bpy, and to +0.97 or +0.98 V, respectively, for 6,6′-Br_2bpy [16]. Multiple ligand-based irreversible reduction processes are observed for the [Cu(P^P)(Br_2phen)][PF_6] compounds (Table 2). This compares to a single reduction process for [Cu(POP)(phen)][PF_6] [11].

Table 2. Cyclic voltammetric data for [Cu(P^P)(N^N)][PF_6] complexes referenced to internal Fc/Fc^+ = 0.0 V; CH_2Cl_2 solutions (ca. 2×10^{-3} mol dm^{-3}) with [^{n}Bu_4N][PF_6] as supporting electrolyte and scan rate of 0.1 V s^{-1}.

Cation in [Cu(P^P)(N^N)][PF_6]	$E_{1/2}{}^{ox}$/V	$E_{pc} - E_{pa}$/mV	I_{pc}/I_{pa}	E_{pc} [a]	$E_{1/2}{}^{red}$/V [b]
[Cu(POP)(2,9-Br_2phen)]$^+$				+0.98	−2.23, −2.10, −1.92, −1.83
[Cu(POP)(3,8-Br_2phen)]$^+$	+0.86	120	0.13		−2.20, −1.94, −1.83
[Cu(POP)(4,7-Br_2phen)]$^+$	+0.79	130	0.12		−2.17, −1.93, −1.84
[Cu(xantphos)(2,9-Br_2phen)]$^+$	+0.97	105	0.19		−2.08, −1.85, −1.74
[Cu(xantphos)(3,8-Br_2phen)]$^+$				+0.87	−2.19, −1.90, −1.81
[Cu(xantphos)(4,7-Br_2phen)]$^+$				+0.95	−2.17, −1.87, −1.77

[a] The value is given for E_{pc} because the process is irreversible. [b] The value is for E_{pa}; the process is irreversible.

2.4. Photophysical Properties

The absorption spectra of CH_2Cl_2 solutions of the copper(I) compounds are shown in Figure 7 and absorption maxima are given in Table 3. The high energy absorptions ($\lambda < 345$ nm) are assigned to ligand-centred, spin-allowed transitions. The broad absorption bands with λ_{max} in the range 415–420 nm (Table 3) arise from metal-to-ligand charge transfer (MLCT). The profile of the absorption spectrum of [Cu(xantphos)(3,8-Br_2phen)][PF_6] is consistent with that reported for the corresponding perchlorate salt [26]. For both the POP- and xantphos-containing complexes, Figure 7 illustrates an increase in values of ε_{max} on going from 2,9-Br_2phen to 3,8-Br_2phen to 4,7-Br_2phen.

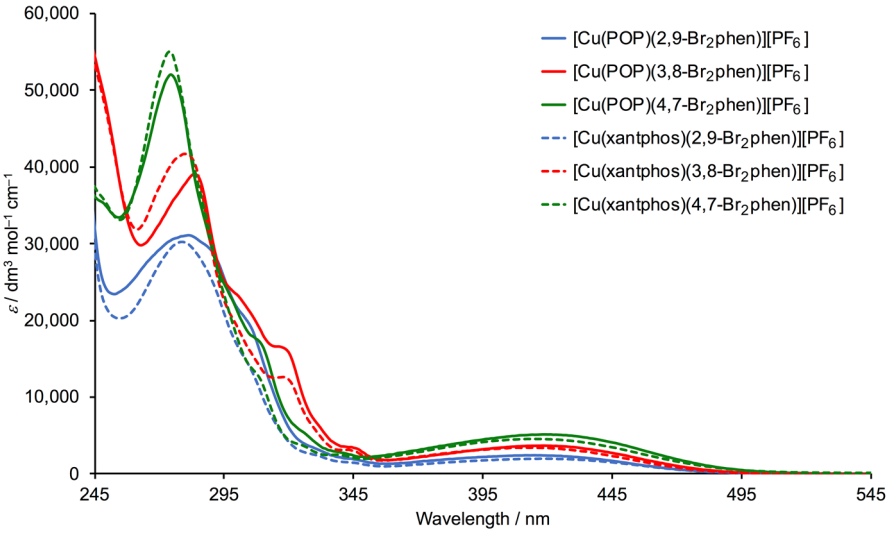

Figure 7. Solution absorption spectra of the [Cu(P^P)(N^N)][PF_6] compounds in CH_2Cl_2 (concentrations in the range 1.75×10^{-5} to 3.0×10^{-5} mol dm^{-3}).

Table 3. Solution absorption maxima for the [Cu(P^P)(N^N)][PF_6] compounds in CH_2Cl_2 (concentrations in the range 1.75×10^{-5} to 3.0×10^{-5} mol dm^{-3}).

Cation in [Cu(P^P)(N^N)][PF_6]	λ_{max}/nm (ε_{max}/dm³ mol⁻¹ cm⁻¹)	
	Ligand-Based Absorptions	**MLCT**
[Cu(POP)(2,9-Br_2phen)]$^+$	281 (31,100), 304 sh (19,800), 346 (2900)	415 (2400)
[Cu(POP)(3,8-Br_2phen)]$^+$	283 (39,100), 302 sh (22,500), 319 sh (16,200), 346 (2900)	418 (3700)
[Cu(POP)(4,7-Br_2phen)]$^+$	274 (52,000), 309 sh (17,000), 327 sh (5000)	418 (5100)
[Cu(xantphos)(2,9-Br_2phen)]$^+$	280 (30,200), 304 sh (19,800), 346 (2900)	415 (2400)
[Cu(xantphos)(3,8-Br_2phen)]$^+$	282 (41,700), 320 sh (12,500), 346 (2900)	416 (3400)
[Cu(xantphos)(4,7-Br_2phen)]$^+$	275 (54,500), 309 sh (12,200), 327 sh (5000)	420 (4500)

When excited into the MLCT region, deaerated CH_2Cl_2 solutions of the copper(I) compounds are weak yellow or orange emitters. Solution emission spectra are displayed in Figure 8 and the emission maxima are given in Table 4. All solution PLQYs were <1%. By analogy with other [Cu(P^P)(N^N)]$^+$ complexes [14], the emissions are assigned to dπ(Cu)→π^*(diimine) (^{3}MLCT) transitions. For [Cu(POP)(2,9-Br_2phen)][PF_6] and [Cu(xantphos)(2,9-Br_2phen)][PF_6], there is a significant blue-shift in the emission ($\lambda_{em}{}^{max}$ = 596 and 582 nm, respectively) compared to the compounds with 3,8-Br_2phen and 4,7-Br_2phen ($\lambda_{em}{}^{max}$ is between 653 and 660 nm). This indicates a higher energy MLCT excited state for the 2,9-Br_2phen-containing complexes and is consistent with the higher oxidation potentials discussed above (Table 2). The emission maxima of 596 and 582 nm for [Cu(POP)(2,9-Br_2phen)][PF_6] and [Cu(xantphos)(2,9-Br_2phen)][PF_6], respectively, are similar to $\lambda_{em}{}^{max}$ = 570 nm for [Cu(POP)(2,9-Me_2phen)][BF_4] in CH_2Cl_2 at room temperature [31]. However,

the solution PLQY of [Cu(POP)(2,9-Me_2phen)][BF_4] of 15% is significantly higher than PLQYs of [Cu(POP)(2,9-Br_2phen)][PF_6] and [Cu(xantphos)(2,9-Br_2phen)][PF_6]. It is well established that the presence of sterically demanding substituents in the phen ligand are critical for suppressing exciplex quenching [31], but the similarities in the crystal structures of [Cu(POP)(2,9-Br_2phen)][PF_6]·Et_2O and [Cu(POP)(2,9-Me_2phen)][PF_6]·Et_2O (see earlier discussion) indicate that steric effects are unlikely to be the cause of the low PLQYs for the 2,9-Br_2phen-containing compounds. It is also worth noting that Pellegrin, Daniel and coworkers reported that solution PLQYs for homoleptic [Cu(2,9-X_2phen)$_2$][PF_6] (X = Cl, Br, I) are higher than that of Cu(2,9-Me_2phen)$_2$][PF_6] and conclude that this is "difficult to rationalize only on steric grounds" [27].

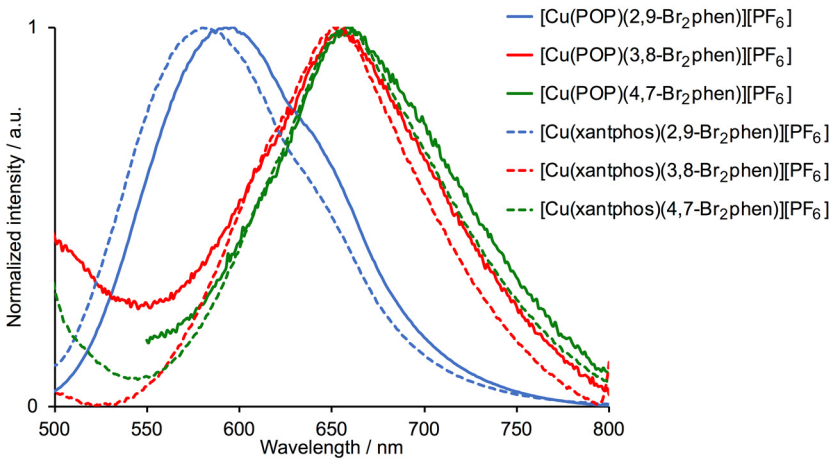

Figure 8. Normalized solution emission spectra of the [Cu(P^P)(N^N)][PF_6] compounds in CH_2Cl_2 (concentration ca. 2.0×10^{-5} mol dm^{-3}). See Table 4 for λ_{exc}.

Table 4. Room temperature solution emission maxima (CH_2Cl_2, ca. 2.0×10^{-5} mol dm^{-3}) and solid-state emission maxima, PLQY values and excited-state lifetimes for the [Cu(P^P)(N^N)][PF_6] compounds.

Cation in [Cu(P^P)(N^N)][PF_6]	Solution		Powder		
	λ_{exc}/nm	$\lambda_{em}{}^{max}$/nm	$\lambda_{em}{}^{max}$/nm [a]	PLQY/%	$\tau_{1/2}$/μs
[Cu(POP)(2,9-Br_2phen)]$^+$	415	596	574	24	6.3
[Cu(POP)(3,8-Br_2phen)]$^+$	420	655	578	3	0.9
[Cu(POP)(4,7-Br_2phen)]$^+$	425	660	604	7	1.7
[Cu(xantphos)(2,9-Br_2phen)]$^+$	425	582	554	45	9.9
[Cu(xantphos)(3,8-Br_2phen)]$^+$	410	653	598	21	8.4
[Cu(xantphos)(4,7-Br_2phen)]$^+$	420	657	580	12	4.2

[a] λ_{exc} = 365 nm for POP-containing compounds; λ_{exc} = 340 nm for xantphos-containing compounds.

Powdered samples of all the [Cu(POP)(N^N)][PF_6] and [Cu(xantphos)(N^N)][PF_6] compounds are yellow or orange emitters when excited at 365 or 340 nm, with values of $\lambda_{em}{}^{max}$ in the range 554–604 nm (Table 4 and Figure 9). The value of $\lambda_{em}{}^{max}$ = 598 nm for [Cu(xantphos)(3,8-Br_2phen)][PF_6] appears to be red-shifted with respect to that reported for solid [Cu(xantphos)(3,8-Br_2phen)][ClO_4] ($\lambda_{em}{}^{max}$ = 565 nm) [26], and may reflect differences in solid-state packing interactions. Each solid-state emission maximum is blue-shifted with respect to solution (Table 4) and this is typical of most other heteroleptic [Cu(P^P)(N^N)]$^+$ complexes [14,16]. As in solution, values of $\lambda_{em}{}^{max}$ for solid-state [Cu(POP)(2,9-Br_2phen)][PF_6] and [Cu(xantphos)(2,9-Br_2phen)][PF_6] are blue-shifted with respect to compounds with the 3,8- and 4,7-isomers, although the effect is less pronounced for the powders. The solid-state PLQY values are highest for the complexes containing the 2,9-Br_2phen ligands (24% for [Cu(POP)(2,9-Br_2phen)][PF_6] and 45% for [Cu(xantphos)(2,9-Br_2phen)][PF_6]) and these values are lower than PLQYs of 66% and 88% for [Cu(POP)(2,9-Me_2phen)][BARF] and [Cu(xantphos)(2,9-Me_2phen)][BARF] ([BARF]$^-$ = tetrakis [3,5-bis(trifluoromethyl)phenylborate]) [32].

For comparison, a PLQY of 36.6% ($\lambda_{em}{}^{max}$ = 566 nm) has been reported for powdered [Cu(POP)(phen)][BF_4] and the excited-state lifetime of 12.75 μs for the latter [11] is similar to $\tau_{1/2}$ = 9.9 μs of [Cu(xantphos)(2,9-Br_2phen)][PF_6]. Thus, the data indicate that the incorporation of the bromo-substituents in the 2,9-positions is less beneficial than the presence of methyl groups.

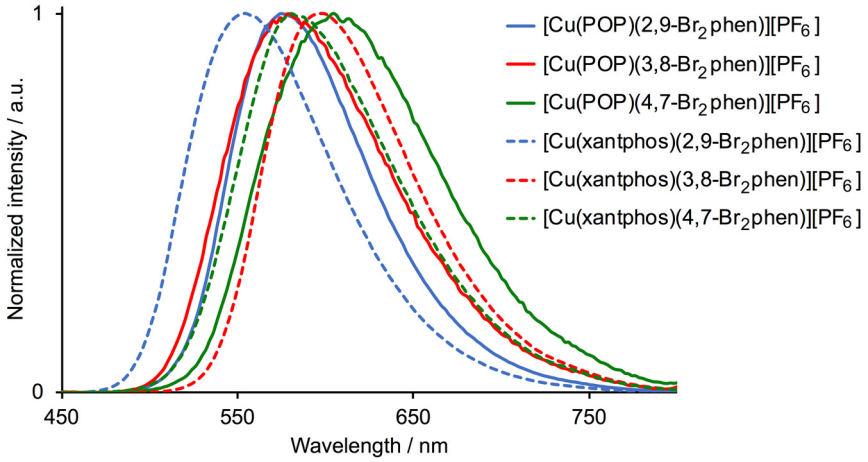

Figure 9. Normalized emission spectra of powder samples of the [Cu(P^P)(N^N)][PF_6] compounds. See Table 4 for λ_{exc}.

3. Materials and Methods

3.1. General

^{1}H, ^{13}C{^{1}H} and ^{31}P{^{1}H} NMR spectra were recorded on a Bruker Avance 500 spectrometer (Bruker BioSpin AG, Fällanden, Switzerland) at 298 K. ^{1}H and ^{13}C NMR chemical shifts were referenced to the residual solvent peaks with respect to δ(TMS) = 0 ppm and ^{31}P NMR chemical shifts with respect to δ(85% aqueous H_3PO_4) = 0 ppm. Solution absorption and emission spectra were measured using a Shimadzu UV2600 spectrophotometer and a Shimadzu RF-5301PC spectrofluorometer, respectively (Shimadzu Schweiz GmbH, Reinach, Switzerland). A Shimadzu LCMS-2020 instrument (Shimadzu Schweiz GmbH) was used to record electrospray (ESI) mass spectra; high resolution ESI (HR-ESI) mass spectra were measured on a Bruker maXis 4G QTOF instrument (Bruker BioSpin AG, Fällanden, Switzerland). Quantum yields (CH_2Cl_2 solution and powder) were measured using a Hamamatsu absolute photoluminescence quantum yield spectrometer C11347 Quantaurus-QY (Hamamatsu Photonics, Solothurn, Switzerland). Powder emission spectra and excited state lifetimes were measured with a Hamamatsu Compact Fluorescence lifetime Spectrometer C11367 Quantaurus-Tau (Hamamatsu Photonics, Solothurn, Switzerland) with an LED light source (λ_{exc} = 340 or 365 nm). Electrochemical measurements used a CH Instruments 900B potentiostat (CH Instruments, Austin, TX, USA) with [^{n}Bu$_4$N][PF_6] (0.1 M) as supporting electrolyte and a scan rate of 0.1 V s^{-1}; the solvent was CH_2Cl_2 and solution concentrations were ca. 2×10^{-3} mol dm^{-3}. The working electrode was glassy carbon, the reference electrode was a leakless Ag^+/AgCl (eDAQ ET069-1) and the counter-electrode was a platinum wire. Final potentials were internally referenced with respect to the Fc/Fc^+ couple.

[Cu(MeCN)$_4$][PF_6] was prepared according to the literature [33]. 3,8-Br_2phen and 4,7-Br_2phen were purchased from Fluorochem (Chemie Brunschwig AG, Basel, Switzerland). 2,9-Br_2phen was prepared following a previously described route [34] and the NMR spectroscopic data matched those reported [34,35]. Other chemicals were purchased from Sigma Aldrich (Sigma Aldrich Chemie GmbH, Steinheim, Germany).

3.2. General Procedures for Copper(I) Compound Synthesis

POP-containing compounds were synthesized according to the following procedure. POP (1.1 eq.) and [Cu(MeCN)4][PF6] (1.0 eq.) were dissolved in CH2Cl2 (20 mL) and the reaction mixture was stirred for 1 h. Then, the N^N ligand (1.0 eq.) was added and the reaction mixture was stirred for 1 h. The solvent was then removed under reduced pressure. The residue was washed with Et2O. The crude product was purified by crystallization from CH2Cl2/Et2O by vapour diffusion.

Compounds containing xantphos were prepared by the following procedure. A solution of the respective phen (1.0 eq.) and xantphos (1.1 eq.) in CH2Cl2 (10 mL) was added dropwise to a CH2Cl2 solution (10 mL) of [Cu(MeCN)4][PF6] (1.0 eq.). The reaction mixture was then stirred for 90 min before the solvent was removed under reduced pressure. The residue was washed with Et2O. The crude product was purified by crystallization from CH2Cl2/Et2O by vapour diffusion.

3.3. [Cu(POP)(2,9-Br$_2$phen)][PF$_6$]

The reagents were POP (106 mg, 0.20 mmol), [Cu(MeCN)$_4$][PF$_6$] (66.5 mg, 0.18 mmol) and 2,9-Br$_2$phen (60.6 mg, 0.18 mmol). [Cu(POP)(2,9-Br$_2$phen)][PF$_6$] was isolated as an orange solid (170 mg, 0.16 mmol, 88%). ^{1}H NMR (500 MHz, acetone-d_6) δ/ppm 8.67 (d, J = 8.5 Hz, 2H, H^{A4}), 8.20 (s, 2H, H^{A5}), 8.11 (d, J = 8.5 Hz, 2H, H^{A3}), 7.46 (ddd, J = 8.3, 6.9, 2.1 Hz, 2H, H^{C4}), 7.37–7.29 (m, 4H, H^{C5+C6}), 7.29–7.24 (m, 4H, H^{D4}), 7.24–7.18 (m, 8H, H^{D2}), 7.16–7.10 (m, 8H, H^{D3}), 7.09–7.06 (m, 2H, H^{C3}). ^{13}C{^{1}H} NMR (126 MHz, acetone-d_6) δ/ppm 159.4 (C^{C1}), 144.2 (C^{A10a}), 144.0 (C^{A2}), 141.3 (C^{A4}), 134.6 (C^{C3}), 134.1 (t, J_{PC} = 7.8 Hz, C^{D2}), 133.2 (C^{C5}), 132.8 (t, J_{PC} = 17.1 Hz, C^{D1}), 131.3 (C^{A3}), 130.6 (C^{D4}), 129.8 (C^{A4a}), 129.3 (t, J_{PC} = 4.7 Hz, C^{D3}), 128.2 (C^{A5}), 126.5 (C^{C2}), 125.9 (t, J_{PC} = 2 Hz, C^{C4}), 120.8 (t, J_{PC} = 2.0 Hz, C^{C6}). ^{31}P{^{1}H} NMR (202 MHz, acetone-d_6, 298 K) δ/ppm −12.8 (POP), −144.2 (septet, J_{PF} = 707 Hz, PF$_6^-$). ESI-MS positive mode *m/z* 939.02 [M − PF6]$^+$ (calc. 938.98), 601.09 [Cu(POP)]$^+$ (calc. 601.09). HR ESI-MS positive mode *m/z* 938.9775 [M − PF6]$^+$ (calc. 938.9784). Satisfactory elemental analytical data could not be obtained.

3.4. [Cu(POP)(3,8-Br$_2$phen)][PF$_6$]

The reagents were POP (297 mg, 0.55 mmol), [Cu(MeCN)$_4$][PF$_6$] (186 mg, 0.50 mmol) and 3,8-Br$_2$phen (168 mg, 0.50 mmol). [Cu(POP)(3,8-Br$_2$phen)][PF$_6$] was isolated as an orange solid (480 mg, 0.44 mmol, 89%). ^{1}H NMR (500 MHz, acetone-d_6) δ/ppm 8.97 (m, 4H, H^{A2+A4}), 8.24 (s, 2H, H^{A5}), 7.46 (ddd, J = 8.9, 7.6, 1.7 Hz, 2H, H^{C5}), 7.35 (m, 4H, H^{D4}), 7.27–7.19 (m, 10H, H^{C6+D3}), 7.17 (m, 8H, H^{D2}), 7.12 (t, J = 7.6 Hz, 2H, H^{C4}), 6.82 (m, 2H, H^{C3}). ^{13}C{^{1}H} NMR (126 MHz, acetone-d_6) δ/ppm 159.1 (t, J_{PC} = 6.0 Hz, C^{C1}), 151.7 (C^{A2}), 142.3 (t, J_{PC} = 1.9 Hz, C^{A10a}), 140.3 (C^{A4}), 135.0 (C^{C3}), 134.1 (t, J_{PC} = 8.2 Hz, C^{D2}), 133.4 (C^{C5}), 131.5 (C^{A4a}), 131.3 (C^{D1}), 131.1 (C^{D4}), 129.6 (t, J_{PC} = 4.9 Hz, C^{D3}), 128.7 (C^{A5}), 126.3 (t, J_{PC} = 2.3 Hz, C^{C4}), 124.4 (t, J_{PC} = 15.4 Hz, C^{C2}), 121.6 (C^{A3}), 121.4 (t, J_{PC} = 2.0 Hz, C^{C6}). ^{31}P{^{1}H} NMR (202 MHz, acetone-d_6, 298 K) δ/ppm −10.1 (POP), −144.2 (septet, J_{PF} = 707 Hz, PF$_6^-$). ESI-MS positive mode *m/z* 938.96 [M − PF6]$^+$ (calc. 938.98), 601.06 [Cu(POP)]$^+$ (calc. 601.09). Found: C 50.79, H 3.40, N 2.56; $C_{48}H_{34}Br_2CuF_6N_2OP_3 \cdot CH_2Cl_2$ requires C 50.26, H 3.18, N 2.39.

3.5. [Cu(POP)(4,7-Br$_2$phen)][PF$_6$]

The reagents were POP (159 mg, 0.30 mmol), [Cu(MeCN)$_4$][PF$_6$] (99.7 mg, 0.27 mmol) and 4,7-Br$_2$phen (90.6 mg, 0.27 mmol). [Cu(POP)(4,7-Br$_2$phen)][PF$_6$] was isolated as an orange solid (270 mg, 0.25 mmol, 93%). ^{1}H NMR (500 MHz, acetone-d_6) δ/ppm 8.88 (d, J = 5.2 Hz, 2H, H^{A2}), 8.52 (s, 2H, H^{A5}), 8.21 (d, J = 5.2 Hz, 2H, H^{A3}), 7.45 (ddd, J = 8.2, 7.5, 1.7 Hz, 2H, H^{C5}), 7.36–7.30 (m, 4H, H^{D4}), 7.24–7.17 (m, 10H, H^{C6+D3}), 7.15–7.09 (m, 10H, H^{C4+D2}), 6.87–6.81 (m, 2H, H^{C3}). ^{13}C{^{1}H} NMR (126 MHz, acetone-d_6) δ/ppm 159.3 (t, J_{PC} = 6.1 Hz, C^{C1}), 151.1 (C^{A2}), 144.8 (t, J_{PC} = 2.1 Hz, C^{A10a}), 135.9 (t, J_{PC} = 1.1 Hz, C^{A4}), 135.1 (C^{C3}), 134.0 (t, J_{PC} = 8.2 Hz, C^{D2}), 133.3 (C^{C5}), 131.6 (t, J_{PC} = 17.2 Hz, C^{D1}), 131.0 (C^{D4}), 130.4 (C$^{A3/A4a}$), 130.3 (C$^{A3/A4a}$), 129.7 (t, J_{PC} = 4.8 Hz, C^{D3}), 127.8 (C^{A5}), 126.1 (t, J_{PC} = 2.3 Hz, C^{C4}), 124.4 (t, J_{PC} = 15.5 Hz, C^{C2}), 121.6 (t, J_{PC} = 2.1 Hz, C^{C6}). ^{31}P{^{1}H} NMR (202 MHz,

acetone-d_6, 298 K) δ/ppm −11.0 (POP), −144.2 (septet, J_{PF} = 708 Hz, PF_6^-). ESI-MS positive mode *m/z* 938.98 $[M - PF6]^+$ (calc. 938.98), 601.11 $[Cu(POP)]^+$ (calc. 601.09). Found: C 50.67, H 3.26, N 2.59; $C_{48}H_{34}Br_2CuF_6N_2OP_3 \cdot CH_2Cl_2$ requires C 50.26, H 3.18, N 2.39.

3.6. [Cu(xantphos)(2,9-Br_2phen)][PF_6]

The reagents were $[Cu(CH_3CN)_4][PF_6]$ (66.3 mg, 0.18 mmol), 2,9-Br_2phen (60 mg, 0.18 mmol) and xantphos (113 mg, 0.20 mmol). [Cu(xantphos)(2,9-Br_2phen)][PF_6] was isolated as a yellow solid (100 mg, 88.8 µmol, 50%). ^{1}H NMR (500 MHz, acetone-d_6) δ/ppm 8.61 (d, J = 8.4 Hz, 2H, H^{A4}), 8.14 (s, 2H, H^{A5}), 8.06 (d, J = 8.4 Hz, 2H, H^{A3}), 7.83 (d, J = 7.6 Hz, 2H, H^{C5}), 7.34–7.24 (m, 14H, $H^{D2+D4+C4}$), 7.16–7.08 (m, 10H, H^{D3+C3}), 1.74 (s, 6H, H^{Me}). $^{13}C\{^1H\}$ NMR (126 MHz, acetone-d_6) δ/ppm 155.8 (C^{C1}), 143.8/143.2 ($C^{A2+A10a}$), 141.2 (C^{A4}), 134.3 (C^{C6}), 134.1 (t, J_{PC} = 7.6 Hz, C^{D2}), 132.1 (t, J_{PC} = 16.84 Hz, C^{D1}), 131.1 (C^{C3}), 130.9 (C^{A3+D4}), 129.8 (C^{A4a}), 129.4 (t, J_{PC} = 4.6 Hz, C^{D3}), 128.8 (C^{C5}), 128.1 (C^{A5}), 126.0 (C^{C4}), 122.6 (C^{C2}), 36.6 ($C^{xantphos\ bridge}$), 29.2 (C^{CMe}). $^{31}P\{^1H\}$ NMR (202 MHz, acetone-d_6, 298 K) δ/ppm −12.2 (xantphos), −144.2 (septet, J_{PF} = 707 Hz, PF_6^-). ESI-MS positive mode *m/z* 979.03 $[M - PF6]^+$ (calc. 979.01), 641.13 $[Cu(xantphos)]^+$ (calc. 641.12). Found: C 54.06, H 3.56, N 2.62; $C_{51}H_{38}Br_2CuF_6N_2OP_3$ requires C 54.44, H 3.40, N 2.49.

3.7. [Cu(xantphos)(3,8-Br_2phen)][PF_6]

The reagents were $[Cu(CH_3CN)_4][PF_6]$ (188 mg, 0.50 mmol), 3,8-Br_2phen (170 mg, 0.50 mmol) and xantphos (173 mg, 0.51 mmol). [Cu(xantphos)(3,8-Br_2phen)][PF_6] was isolated as orange solid (496 mg, 0.44 mmol, 87%). ^{1}H NMR (500 MHz, acetone-d_6) δ/ppm 8.99 (d, J = 2.0 Hz, 2H, H^{A4}), 8.55 (m, 2H, H^{A2}), 8.25 (s, 2H, H^{A5}), 7.95 (dd, J = 7.9 Hz, 1.3 Hz, 2H, H^{C5}), 7.34–7.27 (m, 6H, H^{D4+C4}), 7.14 (m, 8H, H^{D3}), 7.06 (m, 8H, H^{D2}), 6.66 (m, 2H, H^{C3}), 1.87 (s, 6H, H^{Me}). $^{13}C\{^1H\}$ NMR (126 MHz, acetone-d_6) δ/ppm 155.9 (C^{C1}), 151.3 (C^{A2}), 142.4 (C^{A10a}), 140.6 (C^{A4}), 135.0 (C^{C6}), 133.8 (t, J_{Pc} = 8.0 Hz, C^{D2}), 132.2 (C^{C3}), 131.8 (C^{D1}), 131.6 (C^{A4a}), 131.0 (C^{D4}), 129.7 (t, J_{Pc} = 4.8 Hz, C^{D3}), 128.9 (C^{A5+C5}), 126.4 (C^{C4}), 121.7 (C^{A3}), 120.2 (C^{C2}), 37.1 ($C^{xantphos\ bridge}$), 28.7 (C^{CMe}). $^{31}P\{^1H\}$ NMR (202 MHz, acetone-d_6), 298 K) δ/ppm −11.0 (xantphos), −144.2 (septet, J_{PF} = 707 Hz, PF_6^-). ESI-MS positive mode *m/z* 979.00 $[M - PF6]^+$ (calc. 979.01), 641.12 $[Cu(xantphos)]^+$ (calc. 641.12). Found: C 54.28, H 3.55, N 2.49; $C_{51}H_{38}Br_2CuF_6N_2OP_3$ requires C 54.44, H 3.40, N 2.49.

3.8. [Cu(xantphos)(4,7-Br_2phen)][PF_6]

The reagents were $[Cu(CH_3CN)_4][PF_6]$ (64.9 mg, 0.17 mmol), 4,7-Br_2phen (58.8 mg, 0.17 mmol) and xantphos (111 mg, 0.19 mmol). [Cu(xantphos)(4,7-Br_2phen)][PF_6] was isolated as an orange solid (150 mg, 133 µmol, 77%). ^{1}H NMR (500 MHz, acetone-d_6) δ/ppm 8.60 (d, J = 5.2 Hz, 2H, H^{A2}), 8.50 (s, 2H, H^{A5}), 8.22 (d, J = 5.0 Hz, 2H, H^{A3}), 7.90 (dd, J = 7.8 Hz, 1.2 Hz, 2H, H^{C5}), 7.33–7.26 (m, 6H, H^{D4+C4}), 7.14 (m, 8H, H^{D3}), 7.05 (m, 8H, H^{D2}), 6.74 (m, 2H, H^{C3}), 1.81 (s, 6H, H^{Me}). $^{13}C\{^1H\}$ NMR (126 MHz, acetone-d_6) δ/ppm 155.8 (C^{C1}), 150.7 (C^{A2}), 144.8 (C^{A10a}), 136.4/130.7 (C^{A4+A4a}), 135.1 (C^{C6}), 133.6 (t, J_{PC} = 8.0 Hz, C^{D2}), 132.2 (C^{D1}), 132.1 (C^{C3}), 131.0 (C^{D4}), 130.4 (C^{A3}), 129.6 (t, J_{PC} = 4.7 Hz, C^{D3}), 128.9 (C^{C5}), 127.9 (C^{A5}), 126.2 (C^{C4}), 120.3 (C^{C2}), 37.1 ($C^{xantphos\ bridge}$), 28.7 (C^{CMe}). $^{31}P\{^1H\}$ NMR (202 MHz, acetone-d_6, 298 K) δ/ppm −12.4 (xantphos), −144.3 (septet, J_{PF} = 707 Hz, PF_6^-). ESI-MS positive mode *m/z* 979.03 $[M - PF6]^+$ (calc. 979.01), 641.15 $[Cu(xantphos)]^+$ (calc. 641.12). Found: C 54.28, H 3.55, N 2.49; $C_{51}H_{38}Br_2CuF_6N_2OP_3$ requires C 54.44, H 3.40, N 2.49.

3.9. Crystallography

Single crystal data were collected on a Bruker APEX-II diffractometer (Cu Kα radiation) with data reduction, solution and refinement using the programs APEX [36], ShelXT [37], Olex2 [38] and *SHELXL* v. 2014/7 [39], or using a STOE StadiVari diffractometer equipped with a Pilatus300K detector and with a Metaljet D2 source (Ga Kα radiation); the structure was solved using Superflip [40,41] and Olex2 [38]. See Sections 3.10–3.15 for details of the radiation type for each structure. The model was refined with *SHELXL* v. 2014/7 [39]. Structure analysis used Mercury CSD v. 4.1.0 [42,43].

For [Cu(POP)(4,7-Br_2phen)][PF_6]·CH_2Cl_2, SQUEEZE [44] was used to treat the solvent region. All the numbers and formulae were adapted to keep account of the fact that the electrons removed equated to one molecule of CH_2Cl_2 per copper atom. SQUEEZE was also used to treat the solvent regions in [Cu(xantphos)(4,7-Br_2phen)][PF_6]·CH_2Cl_2·0.9Et_2O and [Cu(xantphos)(2,9-Br_2phen)][PF_6]·1.1CH_2Cl_2, and all the numbers and formulae were adapted to account for this.

3.10. [Cu(POP)(2,9-Br_2phen)][PF_6]·0.5Et_2O

$C_{50}H_{39}Br_2CuF_6N_2O_{1.5}P_3$, M_r = 1122.10, yellow block, triclinic, space group $P-1$, a = 15.1949(10), b = 18.5322(12), c = 18.5423(13) Å, α = 107.867(2), β = 104.444(2), γ = 101.088(2)°, V = 4603.2(5) Å^3, D_c = 1.619 g cm^{-3}, T = 130 K, Z = 4, Z' = 2, μ(CuKα) = 4.260 mm^{-1}. Total 38,972 reflections, 16,488 unique (R_{int} = 0.0241). Refinement of 15,466 reflections (1182 parameters) with $I > 2\sigma(I)$ converged at final R_1 = 0.0369 (R_1 all data = 0.0389), wR_2 = 0.0952 (wR_2 all data = 0.0971), gof = 1.028. CCDC 1966898.

3.11. [Cu(POP)(3,8-Br_2phen)][PF_6]·0.8CH_2Cl_2·0.9H_2O

$C_{48.8}H_{37.4}Br_2Cl_{1.6}CuF_6N_2O_{1.9}P_3$, M_r = 1169.20, yellow plate, monoclinic, space group $P2/c$, a = 12.9120(7), b = 14.0896(8), c = 27.1332(13) Å, β = 94.491(2)°, V = 4921.0(5) Å^3, D_c = 1.578 g cm^{-3}, T = 130 K, Z = 4, Z' = 1, μ(CuKα) = 4.797 mm^{-1}. Total 30,196 reflections, 8930 unique (R_{int} = 0.0313). Refinement of 8307 reflections (556 parameters) with $I > 2\sigma(I)$ converged at final R_1 = 0.0870 (R_1 all data = 0.0905), wR_2 = 0.2489 (wR_2 all data = 0.2516), gof = 1.124. CCDC 1966896.

3.12. [Cu(POP)(4,7-Br_2phen)][PF_6]·CH_2Cl_2

$C_{49}H_{36}Br_2Cl_2CuF_6N_2OP_3$, M_r = 1169.97, yellow block, triclinic, space group $P-1$, a = 12.4032(9), b = 18.9805(14), c = 22.0591(17) Å, α = 70.330(3), β = 77.791(3), γ = 87.292(3)°, V = 4777.9(6) Å^3, D_c = 1.626 g cm^{-3}, T = 130 K, Z = 4, Z' = 2, μ(CuKα) = 5.128 mm^{-1}. Total 42,627 reflections, 17,481 unique (R_{int} = 0.0261). Refinement of 16,297 reflections (1135 parameters) with $I > 2\sigma(I)$ converged at final R_1 = 0.0327 (R_1 all data = 0.0350), wR_2 = 0.0817 (wR_2 all data = 0.0834), gof = 1.011. CCDC 1966899.

3.13. [Cu(xantphos)(2,9-Br_2phen)][PF_6]·1.1CH_2Cl_2

$C_{52.1}H_{40.2}Br_2Cl_{2.2}CuF_6N_2OP_3$, M_r = 1218.52, yellow plate, monoclinic, space group $C2/m$, a = 33.3182(16), b = 14.1050(6), c = 11.8205(5) Å, β = 102.059(5)°, V = 5432.5(4) Å^3, D_c = 1.490 g cm^{-3}, T = 130 K, Z = 4, Z' = 0.5, μ(GaKα) = 4.895 mm^{-1}. Total 15,005 reflections, 5607 unique (R_{int} = 0.0515). Refinement of 4802 reflections (417 parameters) with $I > 2\sigma(I)$ converged at final R_1 = 0.0728 (R_1 all data = 0.0863), wR_2 = 0.1853 (wR_2 all data = 0.1973), gof = 1.034. CCDC 1966895.

3.14. [Cu(xantphos)(3,8-Br_2phen)][PF_6]·1.1CH_2Cl_2·0.7Et_2O

$C_{54.9}H_{47.2}Br_2Cl_{2.2}CuF_6N_2O_{1.7}P_3$, M_r = 1270.40, yellow block, triclinic, space group $P-1$, a = 10.1768(8), b = 13.7504(11), c = 20.1505(16) Å, α = 90.204(2), β = 98.120(2), γ = 99.535(2)°, V = 2751.9(4) Å^3, D_c = 1.533 g cm^{-3}, T = 130 K, Z = 2, Z' = 1, μ(CuKα) = 4.597 mm^{-1}. Total 35,742 reflections, 10,241 unique (R_{int} = 0.0264). Refinement of 9939 reflections (728 parameters) with $I > 2\sigma(I)$ converged at final R_1 = 0.0382 (R_1 all data = 0.0391), wR_2 = 0.1093 (wR_2 all data = 0.1101), gof = 1.073. CCDC 1966894.

3.15. [Cu(xantphos)(4,7-Br_2phen)][PF_6]·CH_2Cl_2·0.9Et_2O

$C_{55.6}H_{49}Br_2Cl_2CuF_6N_2O_{1.9}P_3$, M_r = 1276.74, yellow block, triclinic, space group $P-1$, a = 10.9300(4), b = 14.2927(6), c = 19.2894(8) Å, α = 70.366(3), β = 86.491(3), γ = 73.206(3)°, V = 2715.0(2) Å^3, D_c = 1.562 g cm^{-3}, T = 130 K, Z = 2, Z' = 1, μ(GaKα) = 4.864 mm^{-1}. Total 32,020 reflections, 10,645 unique (R_{int} = 0.0795). Refinement of 9958 reflections (624 parameters) with $I > 2\sigma(I)$ converged at final R_1 = 0.0858 (R_1 all data = 0.0904), wR_2 = 0.2317 (wR_2 all data = 0.2384), gof = 1.059. CCDC 1966897.

4. Conclusions

We prepared and characterized a series of [Cu(POP)(Br_2phen)][PF_6] and [Cu(xantphos)(Br_2phen)][PF_6] compounds in which Br_2phen represents the isomers 2,9-Br_2phen, 3,8-Br_2phen and 4,7-Br_2phen. The formation of these heteroleptic compounds was confirmed by mass spectrometry and single-crystal X-ray structures. The solution ^{1}H, ^{13}C{^{1}H} and ^{31}P{^{1}H} NMR spectra of the copper(I) complexes are consistent with the retention of the structures in solution. Each compound undergoes a partially reversible or irreversible copper-centred oxidation, the highest potential being for 2,9-Br_2phen-containing compounds, consistent with bromo-substituents in the 2,9-positions hindering flattening of the copper(I) coordination sphere on oxidation. In solution, the compounds are weak yellow or orange emitters, and values of $\lambda_{em}{}^{max}$ = 596 and 582 nm for [Cu(POP)(2,9-Br_2phen)][PF_6] and [Cu(xantphos)(2,9-Br_2phen)][PF_6] are blue-shifted with respect to those for the complexes containing 3,8-Br_2phen and 4,7-Br_2phen ($\lambda_{em}{}^{max}$ in the range 653 to 660 nm). In the solid state, all six [Cu(POP)(Br_2phen)][PF_6] and [Cu(xantphos)(Br_2phen)][PF_6] complexes are yellow or orange emitters ($\lambda_{em}{}^{max}$ in the range 554 to 604 nm), the highest-energy being the 2,9-Br_2phen-containing complexes. The highest PLQY (45%) is observed for [Cu(xantphos)(2,9-Br_2phen)][PF_6] ($\tau_{1/2}$ = 9.9 μs). Comparisons of the photophysical properties with those of analogous compounds containing phen or 2,9-Me_2phen indicate that the incorporation of the bromo-substituents in the 2,9-positions is not as beneficial as the presence of methyl groups.

Supplementary Materials: The following are available online at http://www.mdpi.com/2304-6740/8/1/4/s1. Figures S1–S7: electrospray mass spectra; Figures S8–S26: ^{1}H NMR spectra and HMQC and HMBC spectra; Figures S27–S33: Cyclic voltammograms.

Author Contributions: Project management, funding acquisition, supervision and manuscript writing, C.E.H.; project management, funding acquisition, supervision, manuscript editing, E.C.C.; project planning, investigation, data analysis, manuscript editing, I.N.; investigation, data analysis, A.K.; N.T.; X-ray crystallography, A.P. All authors have read and agreed to the published version of the manuscript.

Funding: This research was funded by the Swiss National Science Foundation (Grant number 200020_182000).

Acknowledgments: We acknowledge the support of the University of Basel.

Conflicts of Interest: The authors declare no conflict of interest.

References

1. Buckner, M.T.; McMillin, D.R. Photoluminescence from copper(I) complexes with low-lying metal-to-ligand charge transfer excited states. *J. Chem. Soc. Chem. Commun.* **1978**, *17*, 759–761. [CrossRef]
2. Rader, R.A.; McMillin, D.R.; Buckner, M.T.; Matthews, T.G.; Casadonte, D.J.; Lengel, R.K.; Whittaker, S.B.; Darmon, L.M.; Lytle, F.E. Photostudies of 2,2′-bipyridine bis(triphenylphosphine)copper(1+), 1,10-phenanthroline bis(triphenylphosphine)copper(1+), and 2,9-dimethyl-1,10-phenanthroline bis(triphenylphosphine)copper(1+) in solution and in rigid, low-temperature glasses. Simultaneous multiple emissions from intraligand and charge-transfer states. *J. Am. Chem. Soc.* **1981**, *103*, 5906–5912. [CrossRef]
3. Yersin, H.; Czerwieniec, R.; Shafikov, M.Z.; Suleymanova, A.F. TADF Material Design: Photophysical Background and Case Studies Focusing on CuI and AgI Complexes. *ChemPhysChem* **2017**, *18*, 3508–3535. [CrossRef] [PubMed]
4. Leitl, M.J.; Krylova, V.A.; Djurovich, P.I.; Thompson, M.E.; Yersin, H. Phosphorescence versus Thermally Activated Delayed Fluorescence. Controlling Singlet–Triplet Splitting in Brightly Emitting and Sublimable Cu(I) Compounds. *J. Am. Chem. Soc.* **2014**, *136*, 16032–16038. [CrossRef] [PubMed]
5. Czerwieniec, R.; Leitl, M.J.; Homeier, H.H.H.; Yersin, H. Cu(I) complexes—Thermally activated delayed fluorescence. Photophysical approach and material design. *Coord. Chem. Rev.* **2016**, *325*, 2–28. [CrossRef]
6. Costa, R.D.; Ortí, E.; Bolink, H.J.; Monti, F.; Accorsi, G.; Armaroli, N. Luminescent ionic transition-metal complexes for light-emitting electrochemical cells. *Angew. Chem. Int. Ed.* **2012**, *51*, 8178–8211. [CrossRef]

7. Elie, M.; Gaillard, S.; Renaud, J.-L. Luminescent Cationic Copper(I) Complexes: Synthesis, Photophysical Properties and Application in Light-Emitting Electrochemical Cells. In *Light-Emitting Electrochemical Cells: Concepts, Advances and Challenges*; Costa, R.D., Ed.; Springer: Cham, Switzerland, 2017; Chapter 11; pp. 287–327. [CrossRef]
8. Fresta, E.; Costa, R.D. Beyond traditional light-emitting electrochemical cells—A review of new device designs and emitters. *J. Mater. Chem. C* **2017**, *5*, 5643–5675. [CrossRef]
9. Housecroft, C.E.; Constable, C.E. Over the LEC rainbow: Colour and stability tuning of cyclometallated iridium(III) complexes in light-emitting electrochemical cells. *Coord. Chem. Rev.* **2017**, *350*, 155–177. [CrossRef]
10. Alkan-Zambada, M.; Keller, S.; Martínez-Sarti, L.; Prescimone, A.; Junquera-Hernández, J.M.; Constable, E.C.; Bolink, H.J.; Sessolo, M.; Ortí, E.; Housecroft, C.E. [Cu(P^P)(N^N)][PF_6] compounds with bis(phosphane) and 6-alkoxy, 6-alkylthio, 6-phenyloxy and 6-phenylthio-substituted 2,2′-bipyridine ligands for light-emitting electrochemical cells. *J. Mater. Chem. C* **2018**, *6*, 8460–8471. [CrossRef]
11. Leoni, E.; Mohanraj, J.; Holler, M.; Mohankumar, M.; Nierengarten, I.; Monti, F.; Sournia-Saquet, A.; Delavaux-Nicot, B.; Nierengarten, J.-F.; Armaroli, N. Heteroleptic copper(I) complexes prepared from phenanthroline and bis-phosphine ligands: Rationalization of the photophysical and electrochemical properties. *Inorg. Chem.* **2018**, *57*, 15537–15549. [CrossRef]
12. Zhang, Y.; Schulz, M.; Wächtler, M.; Karnahl, M.; Dietzek, B. Heteroleptic diimine-diphosphine Cu(I) complexes as an alternative towards noble-metal based photosensitizers: Design strategies, photophysical properties and perspective applications. *Coord. Chem. Rev.* **2018**, *356*, 127–146. [CrossRef]
13. Keller, S.; Constable, E.C.; Housecroft, C.E.; Neuburger, M.; Prescimone, A.; Longo, G.; Pertegás, A.; Sessolo, M.; Bolink, H.J. [Cu(bpy)(P^P)]$^+$ containing light-emitting electrochemical cells: Improving performance through simple substitution. *Dalton Trans.* **2014**, *43*, 16593–16596. [CrossRef] [PubMed]
14. Keller, S.; Pertegás, A.; Longo, G.; Martinez, L.; Cerdá, J.; Junquera-Hernández, J.M.; Prescimone, A.; Constable, E.C.; Housecroft, C.E.; Ortí, E.; et al. Shine bright or live long: Substituent effects in [Cu(N^N)(P^P)]$^+$-based light-emitting electrochemical cells where N^N is a 6-substituted 2,2′-bipyridine. *J. Mater. Chem. C* **2016**, *4*, 3857–3871. [CrossRef]
15. Fresta, E.; Volpi, G.; Milanesio, M.; Garino, C.; Barolo, C.; Costa, R.D. Novel Ligand and Device Designs for Stable Light-Emitting Electrochemical Cells Based on Heteroleptic Copper(I) Complexes. *Inorg. Chem.* **2018**, *57*, 10469–10479. [CrossRef]
16. Keller, S.; Prescimone, A.; Bolink, H.J.; Sessolo, M.; Longo, G.; Martínez-Sarti, L.; Junquera-Hernández, J.M.; Constable, E.C.; Ortí, E.; Housecroft, C.E. Luminescent copper(I) complexes with bisphosphane and halogen-substituted 2,2′-bipyridine ligands. *Dalton Trans.* **2018**, *47*, 14263–14276. [CrossRef]
17. Yuasa, J.; Dan, M.; Kawai, T. Phosphorescent properties of metal-free diphosphine ligands and effects of copper binding. *Dalton Trans.* **2013**, *42*, 16096–16101. [CrossRef]
18. Costa, R.D.; Tordera, D.; Ortí, E.; Bolink, H.J.; Schönle, J.; Graber, S.; Housecroft, C.E.; Constable, E.C.; Zampese, J.A. Copper(I) complexes for sustainable light-emitting electrochemical cells. *J. Mater. Chem.* **2011**, *21*, 16108–16118. [CrossRef]
19. Brunner, F.; Graber, S.; Baumgartner, Y.; Häussinger, D.; Prescimone, A.; Constable, E.C.; Housecroft, C.E. The effects of introducing sterically demanding aryl substituents in [Cu(N^N)(P^P)]$^+$ complexes. *Dalton Trans.* **2017**, *46*, 6379–6391. [CrossRef]
20. Kaeser, A.; Mohankumar, M.; Mohanraj, J.; Monti, F.; Holler, M.; Cid, J.J.; Moudam, O.; Nierengarten, I.; Karmazin-Brelot, L.; Duhayon, C.; et al. Heteroleptic Copper(I) Complexes Prepared from Phenanthroline and Bis-Phosphine Ligands. *Inorg. Chem.* **2013**, *52*, 12140–12151. [CrossRef]
21. Graber, S.; Doyle, K.; Neuburger, M.; Housecroft, C.E.; Constable, E.C.; Costa, R.D.; Ortí, E.; Repetto, D.; Bolink, H.J. A supramolecularly-caged ionic iridium(III) complex yielding bright and very stable solid-state light-emitting electrochemical cells. *J. Am. Chem. Soc.* **2008**, *130*, 14944–14945. [CrossRef]
22. Bünzli, A.M.; Constable, E.C.; Housecroft, C.E.; Prescimone, A.; Zampese, J.A.; Longo, G.; Gil-Escrig, L.; Pertegás, A.; Bolink, H.J. Exceptionally long-lived light-emitting electrochemical cells: Multiple intra-cation π-stacking interactions in [Ir(C^N)$_2$(N^N)][PF_6] emitters. *Chem. Sci.* **2015**, *6*, 2843–2852. [CrossRef] [PubMed]
23. Casadonte, D.J.; McMillin, D.R. Hindered Internal Conversion in Rigid Media. Thermally Nonequilibrated ^{3}IL and ^{3}CT Emissions from [Cu(5-X-phen)(PPh_3)$_2$]$^+$ and [Cu(4,7-X_2-phen)(PPh_3)$_2$]$^+$ Systems in a Glass at 77 K. *J. Am. Chem. Soc.* **1987**, *109*, 331–337. [CrossRef]

24. Li, X.-L.; Ai, Y.-B.; Yang, B.; Chen, J.; Tan, M.; Xin, X.-L.; Shi, Y.-H. Syntheses, structures and photophysical properties of a series of luminescent copper(I) mixed-ligand complexes. *Polyhedron* **2012**, *35*, 47–54. [CrossRef]
25. Xin, X.-L.; Chen, M.; Ai, Y.-B.; Yang, F.; Li, X.-L.; Li, F. Aggregation-Induced Emissive Copper(I) Complexes for Living Cell Imaging. *Inorg. Chem.* **2014**, *53*, 2922–2931. [CrossRef]
26. Feng, X.-Y.; Xin, X.-L.; Guo, Y.-M.; Chen, L.-L.; Liang, Y.-Y.; Xu, M.; Li, X.-L. Synthesis, structure and solid luminescence of copper(I)–bromodiimine-diphosphine complexes. *Polyhedron* **2015**, *101*, 23–28. [CrossRef]
27. Brown-Xu, S.; Fumanal, M.; Gourlaouen, C.; Gimeno, L.; Quatela, A.; Thobie-Gautier, C.; Blart, E.; Planchat, A.; Riobé, F.; Monnereau, C.; et al. Intriguing Effects of Halogen Substitution on the Photophysical Properties of 2,9-(Bis)halo-Substituted Phenanthrolinecopper(I) Complexes. *Inorg. Chem.* **2019**, *58*, 7730–7745. [CrossRef]
28. Yang, L.; Powell, D.R.; Houser, R.P. Structural variation in copper(I) complexes with pyridylmethylamide ligands: Structural analysis with a new four-coordinate geometry index, τ_4. *Dalton Trans.* **2007**, 955–964. [CrossRef]
29. Yang, L.; Feng, J.-K.; Ren, A.-M.; Zhang, M.; Ma, Y.-G.; Liu, X.-D. Structures, Electronic States and Electroluminescent Properties of a Series of Cu^{I} Complexes. *Eur. J. Inorg. Chem.* **2005**, 1867–1879. [CrossRef]
30. Groom, C.R.; Bruno, I.J.; Lightfoot, M.P.; Ward, S.C. The Cambridge Structural Database. *Acta Cryst.* **2016**, *B72*, 171–179. [CrossRef]
31. Cuttell, D.G.; Kuang, S.-M.; Fanwick, P.E.; McMillin, D.R.; Walton, R.A. Simple Cu(I) Complexes with Unprecedented Excited-State Lifetimes. *J. Am. Chem. Soc.* **2002**, *124*, 6–7. [CrossRef]
32. Smith, C.S.; Branham, C.W.; Marquardt, B.J.; Mann, K.R. Oxygen Sensing by Luminescence Quenching in Crystals of Cu(xantphos)(phen)$^{+}$ Complexes. *J. Am. Chem. Soc.* **2010**, *132*, 14079–14085. [CrossRef] [PubMed]
33. Kubas, G.J.; Monzyk, B.; Crumbliss, A.L. Tetrakis(acetonitrile)copper(I) hexafluorophosphate. *Inorg. Synth.* **1979**, *19*, 90–92. [CrossRef]
34. Guo, H.C.; Zheng, R.H.; Jiang, H.J. Improved Synthesis of 2,9-Dichloro-1,10-phenanthroline. *Org. Prep. Proced. Internat.* **2012**, *44*, 392–396. [CrossRef]
35. Thomas, S.W.; Venkatesan, K.; Müller, P.; Swager, T.M. Dark-field Oxidative Addition-based Chemosensing: New Bis-cyclometalated Pt(II) COmplexes and Phosphorescent Detection of Cyanogen Halides. *J. Am. Chem. Soc.* **2006**, *128*, 16641–16648. [CrossRef] [PubMed]
36. *Software for the Integration of CCD Detector System Bruker Analytical X-ray Systems*; Bruker AXS: Madison, WI, USA, 2013.
37. Sheldrick, G.M. ShelXT-Integrated space-group and crystal-structure determination. *Acta Cryst.* **2015**, *A71*, 3–8. [CrossRef]
38. Dolomanov, O.V.; Bourhis, L.J.; Gildea, R.J.; Howard, J.A.K.; Puschmann, H. Olex2: A Complete Structure Solution, Refinement and Analysis Program. *J. Appl. Cryst.* **2009**, *42*, 339–341. [CrossRef]
39. Sheldrick, G.M. Crystal Structure Refinement with SHELXL. *Acta Cryst.* **2015**, *C27*,, 3–8. [CrossRef]
40. Palatinus, L.; Chapuis, G. Superflip—A Computer Program for the Solution of Crystal Structures by Charge Flipping in Arbitrary Dimensions. *J. Appl. Cryst.* **2007**, *40*, 786–790. [CrossRef]
41. Palatinus, L.; Prathapa, S.J.; van Smaalen, S. EDMA: A Computer Program for Topological Analysis of Discrete Electron Densities. *J. Appl. Cryst.* **2012**, *45*, 575–580. [CrossRef]
42. Macrae, C.F.; Edgington, P.R.; McCabe, P.; Pidcock, E.; Shields, G.P.; Taylor, R.; Towler, M.; van de Streek, J. Mercury: Visualization and Analysis of Crystal Structures. *J. Appl. Cryst.* **2006**, *39*, 453–457. [CrossRef]
43. Macrae, C.F.; Bruno, I.J.; Chisholm, J.A.; Edgington, P.R.; McCabe, P.; Pidcock, E.; Rodriguez-Monge, L.; Taylor, R.; van de Streek, J.; Wood, P.A. Mercury CSD 2.0—New Features for the Visualization and Investigation of Crystal Structures. *J. Appl. Cryst.* **2008**, *41*, 466–470. [CrossRef]
44. Spek, A.L. Platon Squeeze: A Tool for the Calculation of the Disordered Solvent Contribution to the Calculated Structure Factors. *Acta Crystallogr. Sect. C Struct. Chem.* **2015**, *71*, 9–18. [CrossRef] [PubMed]